coatings

MDPI

Article

Influence of Vanadium and Niobium Carbide Particles on the Mechanical, Microstructural, and Physical Properties of AA6061 Aluminum-Based Mono- and Hybrid Composite Using FSP

Waheed Sami Abushanab [1], Essam B. Moustafa [2,*], Emad S. Goda [3], Emad Ghandourah [4], Mohammed A. Taha [5] and Ahmed O. Mosleh [6]

1 Marine Engineering Department, Faculty of Maritime Studies and Marine Engineering, King Abdulaziz University, Jeddah 21589, Saudi Arabia
2 Mechanical Engineering Department, Faculty of Engineering, King Abdulaziz University, Jeddah 80204, Saudi Arabia
3 Gas Analysis and Fire Safety Laboratory, Chemistry Division, National Institute for Standards, 136, Giza 12211, Egypt
4 Department of Nuclear Engineering, Faculty of Engineering, King Abdulaziz University, Jeddah 21589, Saudi Arabia
5 Solid State Physics Department, National Research Centre, El Buhouth St., Dokki, Giza 12622, Egypt
6 Mechanical Engineering Department, Shoubra Faculty of Engineering, Benha University, Cairo 11629, Egypt
* Correspondence: abmostafa@kau.edu.sa

Abstract: The ceramic particle reinforcement process is one of the most utilized techniques to enhance the metal surface. The current investigation uses vanadium and niobium carbides to reinforce the AA6061 alloy using the friction stir process (FSP). The mechanical properties are evaluated using ultrasound and conventional compressive tests; furthermore, the microstructure and physical properties are carried out to show the effect of single and hybrid additives of ceramic particles on the surface composites of aluminum alloy. Scanning electron microscopy (SEM) is utilized to examine the presence and distribution of the reinforcement VC and NbC particles inside the composite matrix. The microstructure examination revealed a good dispersion and homogenized distribution of the reinforcement particles. The results indicated that reinforcement particles significantly enhanced the mechanical and physical properties. The VC and NbC particles play an important role in improving the surface hardening behavior and grain refinement by restricting grain growth during the dynamic recrystallization process in the FSP action. The hybrid composited AA6061/NbC + VC recorded an increase in the compressive stress, yield stress, and hardness of 25%, 20%, and 50%, respectively, relative to the base metal, in addition to a 55% decrease in the coefficient of the thermal expansion (CTE) was reported. Moreover, the hybrid composite AA6061/NbC + VC significantly affected the corrosion rate with a reduction of 45%.

Keywords: hybrid composite; AA6061; corrosion rate; mechanical properties; microstructure; FSP

check for updates

Citation: Abushanab, W.S.; Moustafa, E.B.; Goda, E.S.; Ghandourah, E.; Taha, M.A.; Mosleh, A.O. Influence of Vanadium and Niobium Carbide Particles on the Mechanical, Microstructural, and Physical Properties of AA6061 Aluminum-Based Mono- and Hybrid Composite Using FSP. *Coatings* **2023**, *13*, 142. https://doi.org/10.3390/coatings13010142

Academic Editor: Heping Li

Received: 17 December 2022
Revised: 3 January 2023
Accepted: 9 January 2023
Published: 10 January 2023

Copyright: © 2023 by the authors. Licensee MDPI, Basel, Switzerland. This article is an open access article distributed under the terms and conditions of the Creative Commons Attribution (CC BY) license (https://creativecommons.org/licenses/by/4.0/).

1. Introduction

Aluminum matrix composites, or AMMCs, have found various applications in modern engineering due to their exceptional mechanical properties. In recent years, nanocomposite metal matrices have gained prominence in developing technologies due to their superior performance under various loads and their impact on the environment. The quality of the metal matrix composite can be increased by adding reinforcing particles with distinct properties according to the required improvement [1–3]. Many researchers used the hybridization of nanoparticles with aluminum alloys due to the remarkable properties of the composites. Many researchers have used the hybridization of nanoparticles with aluminum alloys due to the remarkable properties of the composites produced by this process. A composite material with exceptional strength, homogeneity, and refined grains

can be produced by friction stir processing (FSP), stir casting, powder metallurgy, and laser melting [4–9]. FSP is one of the most promising new technologies for improving the properties of metal surfaces. This makes the FSP method one of the most successful for creating metal matrix composite surfaces. Therefore, nanofabrication using FSP is the preferred approach for creating nanocomposite surfaces because it is a safe, versatile, and efficient alternative to obtaining homogenized composites [10–18]. The most challenging part of the FSP process is determining the best processing parameters, including rotation speed, tool design, and traverse speed. According to the required AMMC properties, the reinforcement is added to the metal matrix; for example, FSP was used to produce highly wear-resistant AA6061/B_4C composite surfaces; thus, after numerous machining passes, the refined microstructure grains exhibited exceptional wear resistance [19].

The influence of reinforcement particles, such as VC, SiC, NbC, Al_2O_3, BN, B_4C, etc., on the hardness and mechanical properties of the monocomposite or hybrid composite metal matrix composites, were studied. [18,20]. Incorporating hexagonal boron nitride HBN nanoparticles into aluminum alloys improves the materials' wear resistance, hardness, and mechanical properties [21–23]. Mono-composites have the disadvantage of improving many properties because, rationally speaking, they only focus on improving one or two properties at most [24–27]. For this reason, many researchers have developed hybrid metal matrix composites using more than one reinforcement particle to increase their mechanical properties, as well as increase any property that they would like to add to the new composite, depending on the type of reinforcement particles that have been hybridized with the metal matrix [28,29]. Despite the extensive research, few direct comparisons have been made between the many different reinforcement components that strengthen the aluminum matrix [30–33]. The economic significance of transition metal carbides such as HfC, TiC, VC, and TaC cannot be overstated [34]. This is owing to the very high hardness of these transition metal carbides and the fact that they are beneficial in creating materials resistant to wear [35,36]. It may be used as a material for high-temperature structural applications as a consequence of its high-temperature strength as well as its corrosion resistance. Binary metal carbides may be used as reinforcing particles in aluminum matrix composites due to their strong microhardness values [37].

Regarding high-performance structural materials, transition-metal aluminides such as Al_3Ti, Al_3V, and Al_3Nb, along with other chemically analogous compounds, are among the most attractive possibilities [38]. This is because these compounds exhibit extraordinary mechanical characteristics, which explains why this is the case. Intermetallic compounds embedded in an aluminum matrix formed of Al-Ti, Al-Ta, Al-Nb, Al-V, and Al-Mo can narrow the gap between the thermal expansion coefficients of the reinforcements and matrix [39]. Therefore, the current work is focused on the fabrication of a mono and a hybrid composite of two hard ceramic particles, such as vanadium and niobium carbides, in order to increase the hardness and mechanical properties of the fabricated composites using the friction stirring technique. On the other hand, we investigate the feasibility of two reinforcing particles that have the same effect on the mechanical properties, corrosion behavior and thermal expansion and whether they change the properties of the new composite when hybridized or not.

2. Materials and Methods

This work used sheets of AA6061 aluminum alloy as the base matrix. The chemical composition of the used sheet is listed in Table 1.

Table 1. Chemical composition of the base matrix aluminum alloy, AA6061.

Si	Mg	Cu	Fe	Cr	Al
0.65	1.1	0.28	0.55	0.25	remain

NbC and VC were used as reinforcement particles to strengthen the AA6061 aluminum base matrix in the form of mono and hybrid particles. The reinforcement particles were characterized by transmission electron microscopy (TEM) (JEOL JSM-200F, Tokyo, Japan). The micro/nanostructures of the reinforcement particles are shown in Figure 1. The average particle sizes of VC and NbC are 0.72 ± 0.4 µm and 0.6 ± 0.11 µm, respectively. The friction stir processing (FSP) technique incorporated the hybrid reinforcement particles. Figure 2 illustrates the procedures of the experimental work. Before the FSP, liner hole patterns were milled on the surface of the AA6061 aluminum sheets. The mono particles were filled into the holes directly. For hybrid reinforcement particles, the particles with 50% by volume of NbC and 50% by volume of VC were well mixed for good distribution and homogenization, then filled into the holes. Using an automatic milling machine, (Bridgeport, Elmira, NY, USA) the FSP was carried out at a tool rotation speed of 900 rpm, a traveling speed rate of 30 mm/minute, and a tilt angle of 1°. The taper triangle tool was used for this process. After the FSP, samples were sliced for characterization (microstructure, mechanical, and physical). For microstructure analysis, the as-received and as-processed samples were mechanically grinded by SiC papers, polished, and then etched by metallurgical standard agents. Olympus BX51 optical microscopy (Melville, NY, USA) and JEOL scanning electron microscopy (TEM, JEOL, Tokyo, Japan) were used for microstructure analysis. The grain size is calculated according to [40] line intercept theory. Archimedes' method was carried out to measure both bulk densities. The thermal expansion of AA6061 and its composites was measured with a Netzsch DIL 402 PC (Germany) using a heating rate of 5 °C/min and 30–400 °C rectangular bars. The value of the coefficient of thermal expansion (CTE) is the change in length over the change in temperature

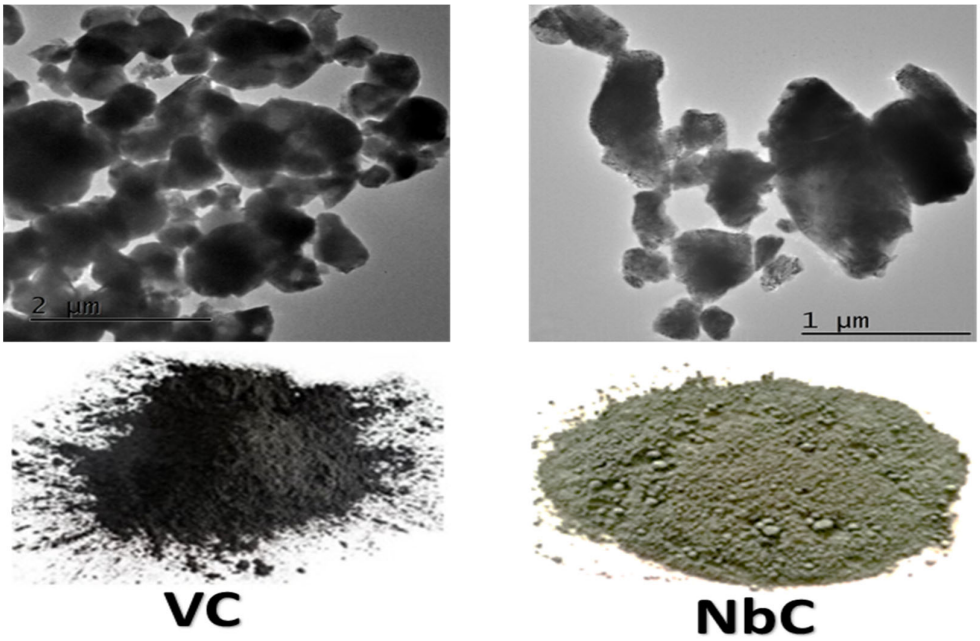


Figure 1. TEM images and corresponding typical powder of the reinforcement particles.

Vickers micro-hardness was measured across all processing regions to illustrate the Vickers micro-hardness profiles. On the ZwickRoell microhardness tester (Zwick/Roell, Kennesaw, GA, USA), Vickers micro-hardness tests were performed according to the ASTM E-384-17 standard with a 100 g load and a 10 s shutter speed. The corrosion test was performed according to ASTM Laboratory Immersion Corrosion Testing of Metals (G 31–72); the following equation can be used to calculate the average corrosion rate:

$$\text{corrosion rate} = K \times W/A \times T \times D$$

where the corrosion rate is in g/cm^{2}h, K = 0.1 (if the corrosion rate is calculated in g/cm^{2}h), and W = weight loss in g; this was performed by subtracting the final weight measured from the initial weight, which gave the weight loss (weight difference), D = density of each sample in g/cm^3, A = area, the area of each sample was determined by calculating the total surface area in cm^2, and T = time, which was the exposure time in hours that each of the samples spent inside the different concentrations of the acidic media.

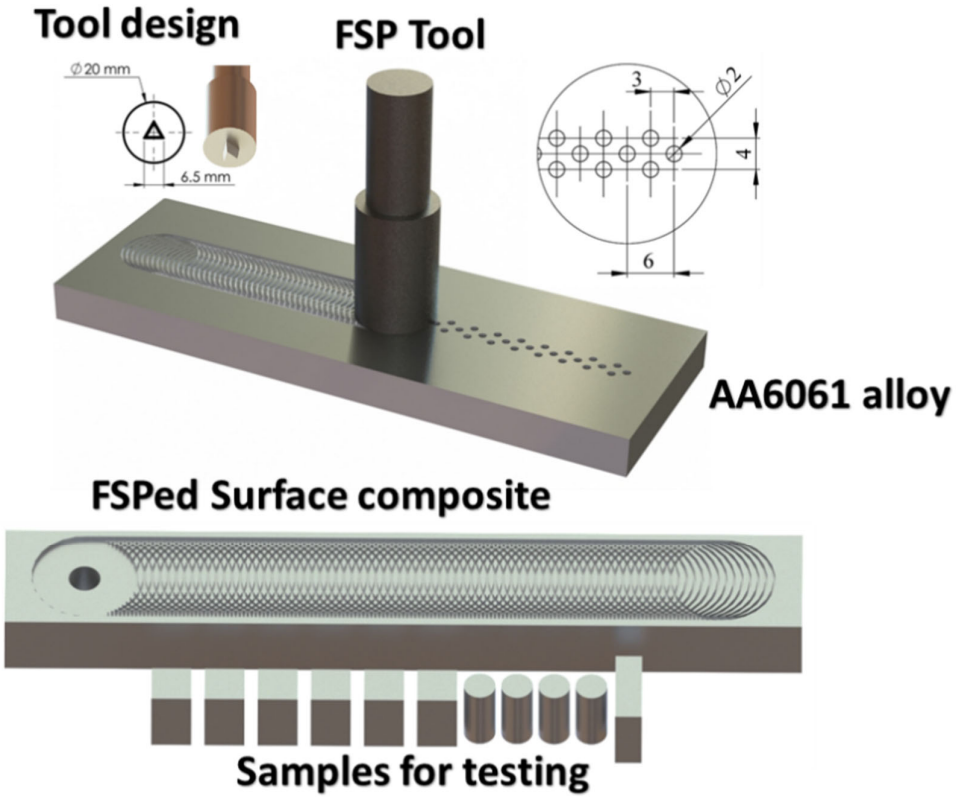


Figure 2. The schematic draw of the FSP process, tool design, and sample location; all dimensions in mm.

3. Results and Discussion

3.1. Microstructure Analysis

Figure 3 shows the optical microscopic images of the as-received rolled AA6061 alloy sheets and the manufactured composites. The microstructure of the as-received sheets exhibits elongated grains in the rolling direction, with an average grain size of 310 µm. The manufactured mono and hybrid composites have refined microstructure grains due to the FSP. The semi-solid thermomechanical deformation due to the FSP led to full recrystallization of the grains in the stirred zone, resulting in finely equiaxed grains. The Zenner pinning effect due to the macro/nanoparticles added more fining effects to the grains, which restricted grain growth after recrystallization. Table 2 shows the calculated grain size and aspect ratio inside the stirred zone, for example average grain size of the AA6061/NbC was 12 µm (Figure 3b), while the averages for the AA6061/VC and the AA6061/NbC + VC were 11.3 µm, 10.5 µm, respectively (Figure 3c,d).

The as-rolled sheets have elongated grains with an aspect ratio of 3.87, which means the grain's length is greater than the thickness by 387.5%. In contrast, the manufactured composites exhibit typically equiaxed strain structures in the stirred zone with a difference between the length and thickness of the grain not exceeding 4%.

The SEM microstructure image of the fabricated mono-composites and the energy dispersive spectrometry (EDS) maps of the manufactured hybrid composite AA6061/NbC+VC are shown in Figure 4; hence the yellow rectangle contain all elemental map image . The

SEM microstructure image shows the good distribution of the reinforced particles by the FSP approach. The EDS maps of the different particles confirm the uniform distribution. The uniform distribution of these particles helped increase the grain's refining in the stirred zone. Moreover, the non-agglomeration of the reinforcement particles should positively affect the properties of the manufactured particles. The ceramic particles of the NbC and VC shown in the SEM images were white due to the reflection of the SEM electron; thus, some agglomeration of the reinforcement particles was found due to the density difference between the base AA6061 alloy and them. However, the FSP process overcomes the major agglomeration of these particles but still retains some residuals in the composite matrix.

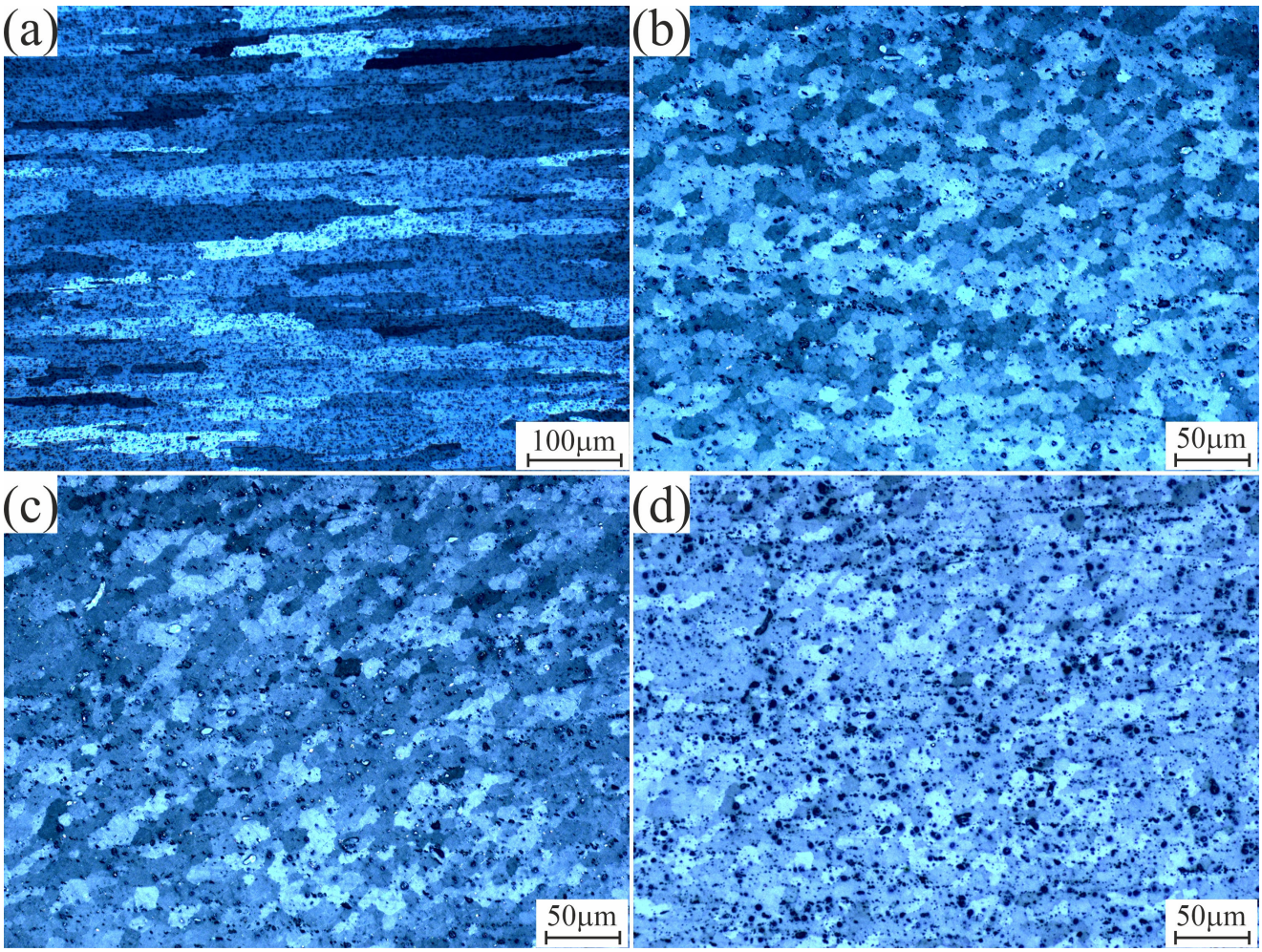


Figure 3. The microstructure of the as-received AA6061 alloy sheets and the manufactured composites; (**a**) as-received alloy sheets, (**b**) AA6061/NbC, (**c**) AA6061/VC, and (**d**) AA6061/NbC + VC.

Table 2. Microstructure grain size inside the stirred zone.

Alloy	Grain Size	Aspect Ratio
AA6061	310	310/80 = 3.87
AA6061/NbC	12	12/11.9 = 1.01
AA6061/VC	11.3	11.3/10.8 = 1.04
AA6061/NbC + VC	10.5	10.5/10.3 = 1.02

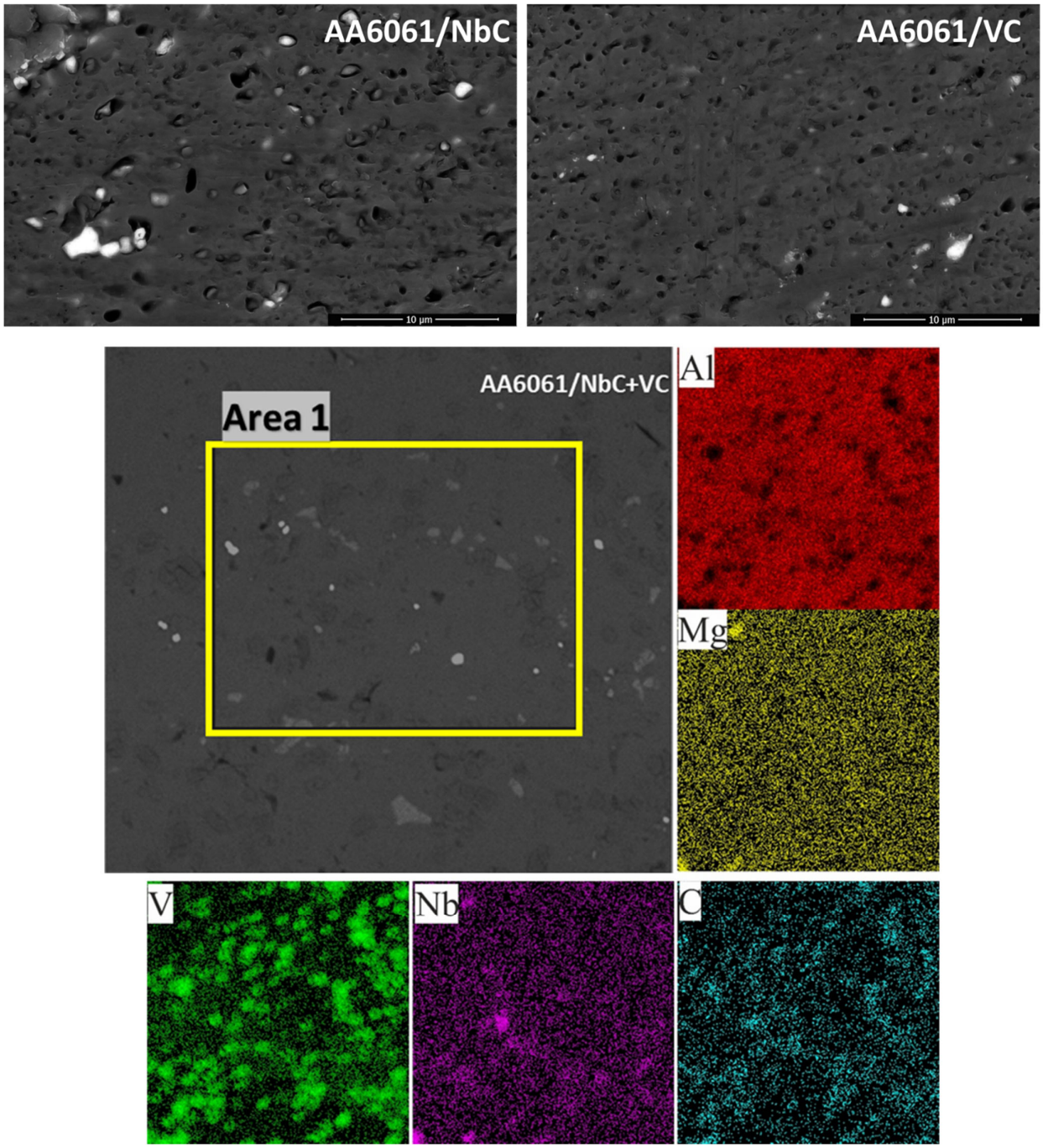


Figure 4. SEM microstructure of the mono-composites AA6061/NbC and AA6061/VC, and the EDS maps of the manufactured hybrid composite AA6061/NbC + VC.

3.2. Thermal Expansion Behavior

The relative thermal expansion (Δl/l) behavior of the AA6061 alloys and composites samples in the temperature range of 30–400 °C is shown in Figure 5. In the specified temperature range, the unreinforced AA6061 alloy matrix has a higher Δl/l range of 0.55×10^{-3} to 9.13×10^{-3} compared with 0.38×10^{-3} to 7.52×10^{-3}, 0.30×10^{-3} to 7.22×10^{-3}, and 0.19×10^{-3} to 4.81×10^{-3} for the composite that contains NbC, VC, and NbC + VC, respectively. Figure 6 shows the changes in CTE of the samples calculated from the slope of the thermal expansion curve. It can be observed that the reinforced carbide particles cause a reduction in CTE values.

The CTE value of AA6061 alloy is 23.2 × 10^{-6}/°C, while this value decreased to 19.8 × 10^{-6}, 18.2 × 10^{-6} and 15.1 × 10^{-6}/°C for composites AA6061/NbC, AA6061/VC, and AA6061/NbC + VC, respectively. As expected, adding ceramic particles into the aluminum alloy matrix significantly reduces the CTE of composite samples. This result is confirmed by the fact that the CTE of reinforcements (NbC and VC = 7.8 and 7.3 × 10^{-6}/°C, respectively) is lower than that of the Al alloy matrix (23.5 × 10^{-6}/°C). In this way, the thermal expansion of Al alloy is effectively constrained, providing good enhancement for the dimensional stability of the Al alloy matrix [41]. On the other hand, adding ceramic reinforcements to Al alloy causes residual stresses in the matrix due to a mismatch of the CTE values between the AA6061 alloy matrix and reinforcements particles. The thermal stresses arising in the Al alloy matrix lead to plastic deformation in the matrix; subsequently, it has an important role in improving the strength of composites [42].

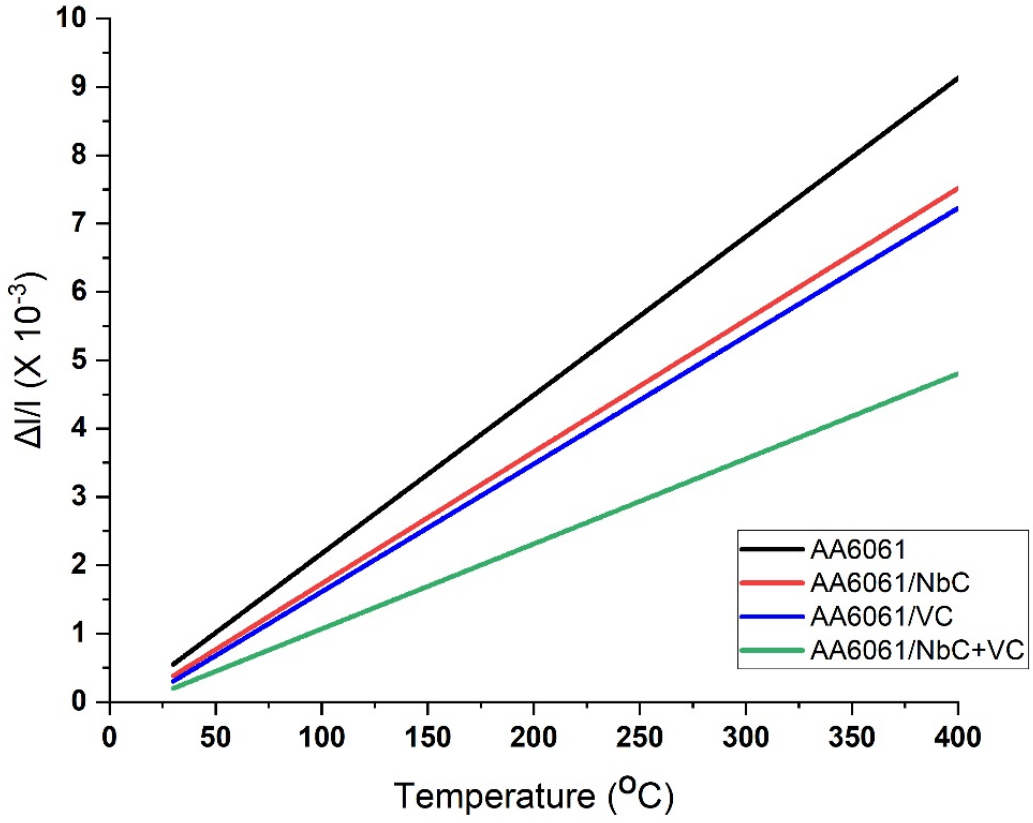


Figure 5. Thermal expansion behavior of Al 6061 and composite samples.

Figure 7 shows the bulk density of the AA6061 alloy and composite samples prepared by the FSP process. It can be seen that the bulk density of various composites is higher than the density of aluminum. It is known that the theoretical density of the AA6061 alloy is about 2.73 g/cm^3, while the densities of NbC and VC are 7.82 and 5.77 g/cm^3, respectively. Therefore, this increase in density will cause an increase in the composite matrices. On one hand, the large difference in melting temperatures between AA6061 alloy (650 °C) and NbC and VC reinforcement (3500 and 2810 °C) reduces particle rearrangement during the FSP method [39]. On the other hand, adding ceramic reinforcements to the Al alloy causes residual stresses in the matrix due to a mismatch in the CTE values between the AA6061 alloy matrix and the reinforcement particles. The thermal stresses arising in the Al alloy matrix lead to plastic deformation in the matrix; consequently, it has an important role in improving the strength of composites

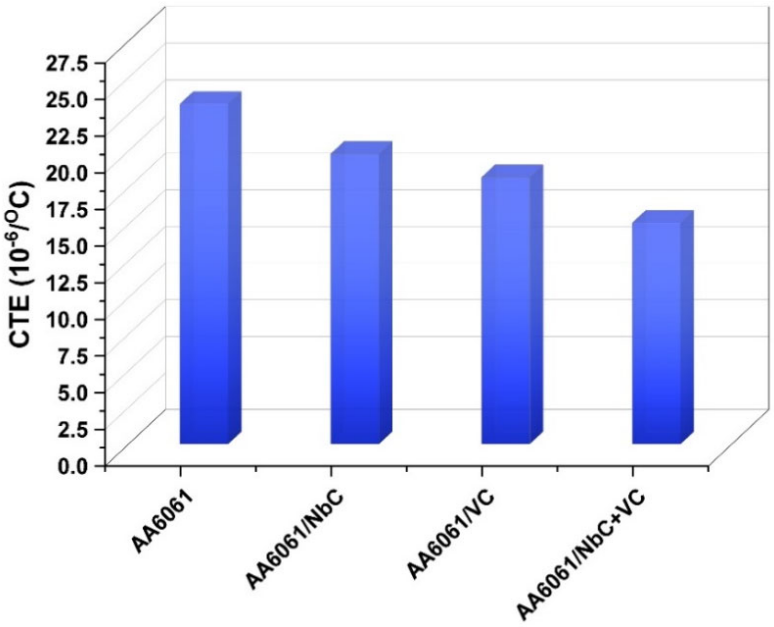


Figure 6. The CTE value of the investigated samples.

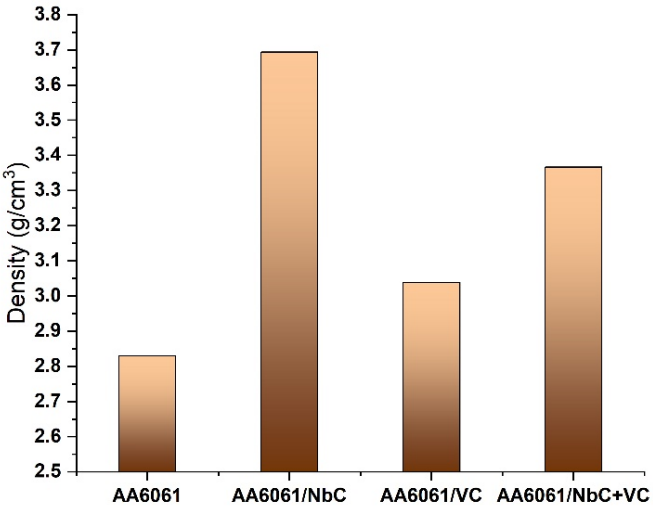


Figure 7. The bulk density of the samples.

The results reveal that adding single and hybrid ceramic nanoparticles to the AA6061 matrix contributes to a positive increase in the elastic moduli of composite samples, as illustrated in Table 3. For AA6061 alloy, the values of longitudinal modulus and share modulus are 96 and 24.4 GPa, respectively, while for AA6061/NbC composites, their increases to 106.2 and 26.9 GPa have improved by about 10.6 and 10.2%, respectively, as shown in Figure 8. Furthermore, AA6061/VC composites increased to 111.3 and 28.2 GPa, with an improvement of 16.5 and 15.6%, respectively. It is worth mentioning that adding a hybrid of reinforcement leads to a noticeable improvement in the values of elastic moduli; for example, the longitudinal modulus improves by about 24.7% compared to the aluminum alloy and also increases by about 12.7 and 7.5% compared to the composites containing NbC, VC, respectively.

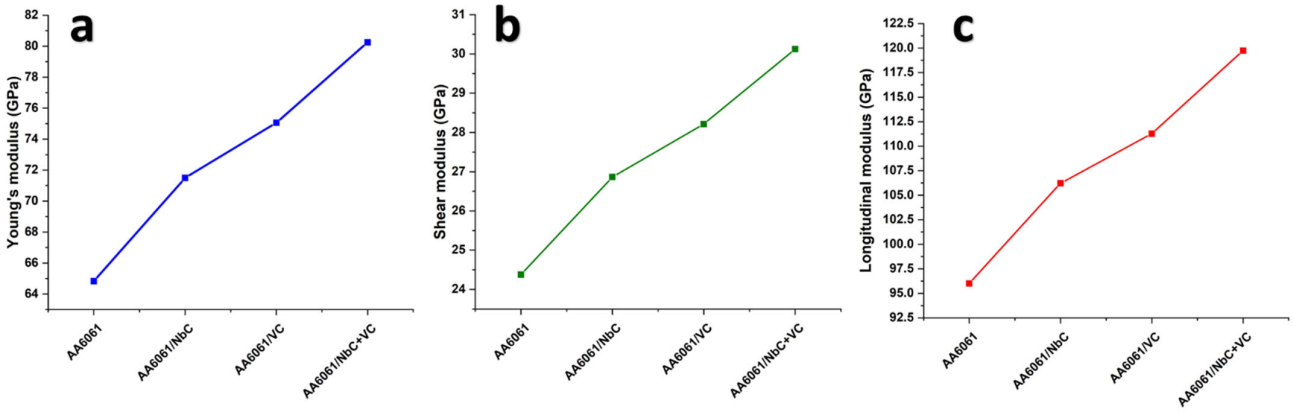


Figure 8. Mechanical properties of the composite samples using ultrasonic measurement (**a**) Young's modulus, (**b**) shear modulus, (**c**) longitudinal modulus.

Table 3. Mechanical properties obtained from an ultrasound test.

	Longitudinal Velocity (VL) m/s	Shear Velocity (VS) m/s	Young's Modulus GPa	Longitudinal Modulus GPa	Bulk Modulus GPa	Shear Modulus GPa
AA6061	5930.12	2988.1	64.83	96.00	71.63	24.38
AA6061/NbC	6737.72	3388.3	71.50	106.23	79.36	26.86
AA6061/VC	6644.78	3346.1	75.06	111.27	83.05	28.21
AA6061/NbC + VC	7048.81	3535.4	80.24	119.74	89.62	30.12

Figure 9 shows the compressive behavior curves of AA6061 different prepared composites. In general, it is clear that the addition of ceramics to the AA6061, whether mono or hybrid, causes an improvement in compressive strength and yield strength, accompanied by some decrease in elongation, which is consistent with much literature [43–45]. The compressive strengths of AA6061/NbC, AA6061/VC, and AA6061/NbC + VC composites are 363.4, 380.2, and 401.8 MPa, respectively, enhanced by about 9, 14, and 22%, respectively, compared with unreinforced AA6061 alloy (333.32 MPa). It should be highlighted that adding VC reinforcement particles has a more substantial effect on increasing strength than adding NbC reinforcement particles. This is due to the superior mechanical characteristics of VC particles compared to NbC particles, which account for their substantial influence. This marked improvement is due to two strengthening contributions, NbC and VC particles, which can be coupled in the hybrid composite to increase mechanical properties effectively. The improvements in the mechanical properties are listed in Table 4.

Table 4. The improvement of the mechanical properties with respect to the base metal (%).

Composite	Compressive Stress	Yield Stress	Young's Modulus	Hardness
AA6061/NbC	9	6	9	27
AA6061/VC	15	9	15	34
AA6061/NbC + VC	25	20	25	50

These mechanical properties, such as compressive strength and elastic moduli of the composites, are improved due to several reasons:

The uniform distribution and closer packing of the ultra-hard ceramics in AA6061, offering greater resistance to plastic deformation, are important in improving mechanical properties.

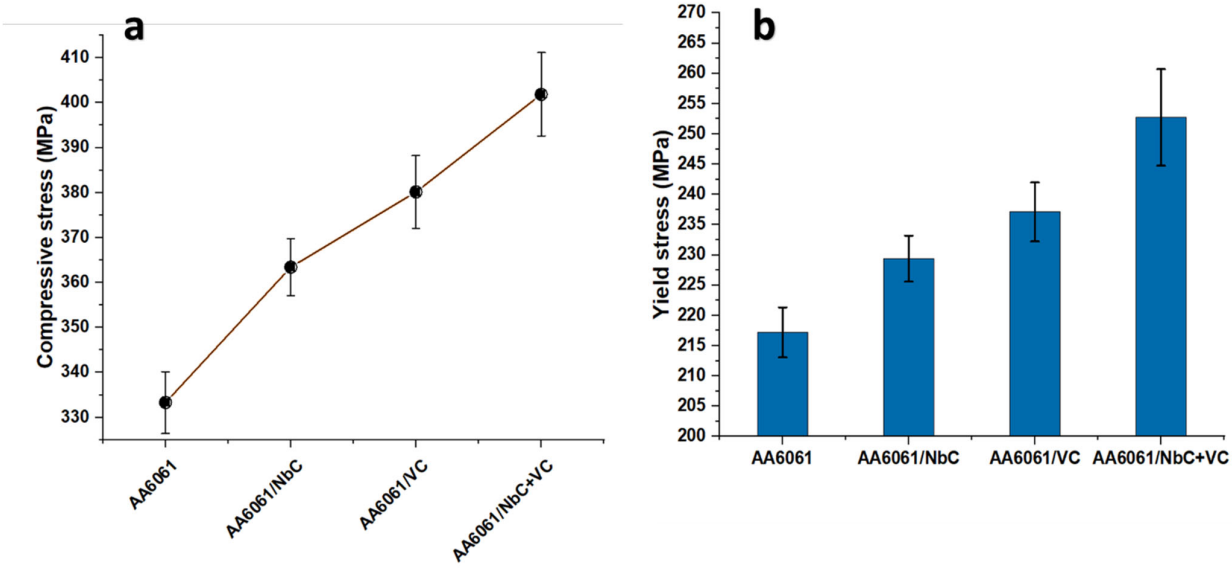


Figure 9. Mechanical properties obtained from compressive test (**a**) ultimate compressive stress, (**b**) yield stress.

The dispersion of ceramics, whether NbC or VC or both, can act as barriers to the movement of the dislocations in the AA6061 alloy, known as Orowan strengthening.

The presence of hard reinforcement transfers the applied load from the AA6061 alloy to the reinforcement (NbC or VC particles) and increases the resistance to plastic deformation of prepared composites. This occurs because the CTE of AA6061 is higher than the CTE of NbC and VC reinforcement particles (6.7 and 7.2 $\times$ 10^{-6}/°C, respectively) and, therefore, there is more thermal stress generated in the composites, which causes dislocations to occur at the boundary between matrix and reinforcement [46].

3.3. Corrosion Behavior

The variation of the weight loss due to the corrosion rate of AA6061 and composites with the exposure time of 1 M HCl solution at room temperature (28 °C) is illustrated in Figure 10. Generally, the results indicate that all samples' weight loss and corrosion rate decreased with increasing exposure time. The corrosion rate of the base AA6061 alloy immersed for 24 h has been observed at 3.3 $\times$ 10^{-5} g/cm^{2}h, and for AA6061/VC, AA6061/NbC, and AA6061/ NbC + VC composites, it is 2.7 $\times$ 10^{-5}, 2.6 $\times$ 10^{-5}, and 2.2 $\times$ 10^{-5} g/cm^{2}h, respectively. Thus, the corrosion rate decreased with the addition of ceramic particles; the total improvement in the corrosion rate was 19.8%, 21.8%, and 33.7%, respectively. For 7 days immersed, the corrosion rates of AA6061 alloy and composite specimens (AA6061/VC, AA6061/NbC, and AA6061/ NbC + VC) decreased to 7.7 $\times$ 10^{-6}, 6.3 $\times$ 10^{-6}, 6.2 $\times$ 10^{-6} and 5.5 $\times$ 10^{-6} g/cm^{2}h, respectively.

These results indicate that when the exposure time is prolonged, the corrosion resistance (corrosion rate decreases) of AA6061 and composites increases as well, due to some passivation of the matrix alloy. It is also clear that the composites had better corrosion resistance than the unreinforced Al alloy, as reflected by the lower weight loss of the composites [47]. This is due to ceramic reinforcement particles on the composite surface, which protect the surface layer in an acidic environment. The corrosion rate of aluminum alloy has improved after adding ceramic reinforcement.

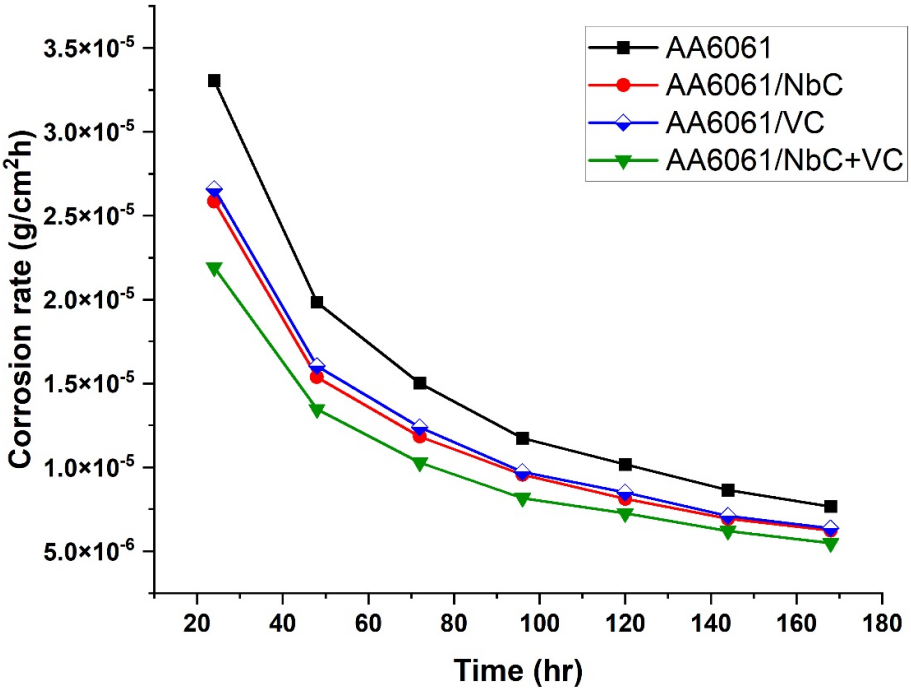


Figure 10. The corrosion rate of the investigated samples against the immersed time in hours.

3.4. Hardness Behavior

The hardness profiles of aluminum surface composites using mono and hybrid reinforcement particles utilizing the FSP are shown in Figure 11. It is evident that the microhardness tends to increase as particle dispersion increases. FSP evenly diffused the presence of hard ceramic particles (NbC) and (VC) over the aluminum surface. The microhardness of the agitated zone or composite surface is much greater than that of the AA6061 alloy substrate. The diminution in particle size is a significant contributor to this improved hardness. According to the Hall–Petch connection [48], a metallic material's grain size substantially impacts its mechanical characteristics, particularly its strength and hardness [49]. According to the same theory, reducing grain structure in freshly formed aluminum composites due to friction stirring and particle dispersion may be the primary cause of the rise in hardness values. The grain size of the AA6061 aluminum alloy surface hybrid composites in the stirring zone is smaller than that of the base alloy due to the grain refining impact of dispersed NbC and VC particles, which raises the microhardness value of the surface composites. The impact of the preceding procedure grows as the number of dispersed reinforcements increases. Moreover, when the dispersion of the reinforcement particles grows, the distance between the ceramic particles reduces, hence decreasing the dislocation motion. This reduction in dislocation motion boosts the microhardness of the generated surface composites. The average microhardness values for the base metal, mono (VC and NbC)- and hybrid (VC + NbC)- composites in the SZ are 81 $\pm$ 2, 102 $\pm$ 2, 107 $\pm$ 3, and 118 $\pm$ 3 HV, respectively. The overall microhardness value at the stirred zone of the mono-composite AA6061/NbC and AA6061/VC increased more than the base alloy by 27 and 34%, respectively (Table 4). These results ensure the main role of the VC particles in the strength of the surface composite reinforcement process. The total microhardness behavior indicated that the AA6061/NbC + VC hybrid composite obtained the greatest improvement, surpassing the AA6061 base alloy by 50% (Table 4). This increase in hardness makes this hybrid composite one of the finest options for applications requiring extensive surface hardening, such as those in the automobile sector.

The significant improvement in the hardness of the SZ for the manufactured composites can be attributed to the presence of the hard ceramic particles. The smoothness in the hardness profile across the SZ confirmed the uniform particle distribution along the SZ.

Particularly, VC exhibits a high hardness greater than the NbC; thus, the composite with VC should exhibit higher hardness values in the stirred zone. Therefore, the nature of the particles played a great role in increasing the hardness

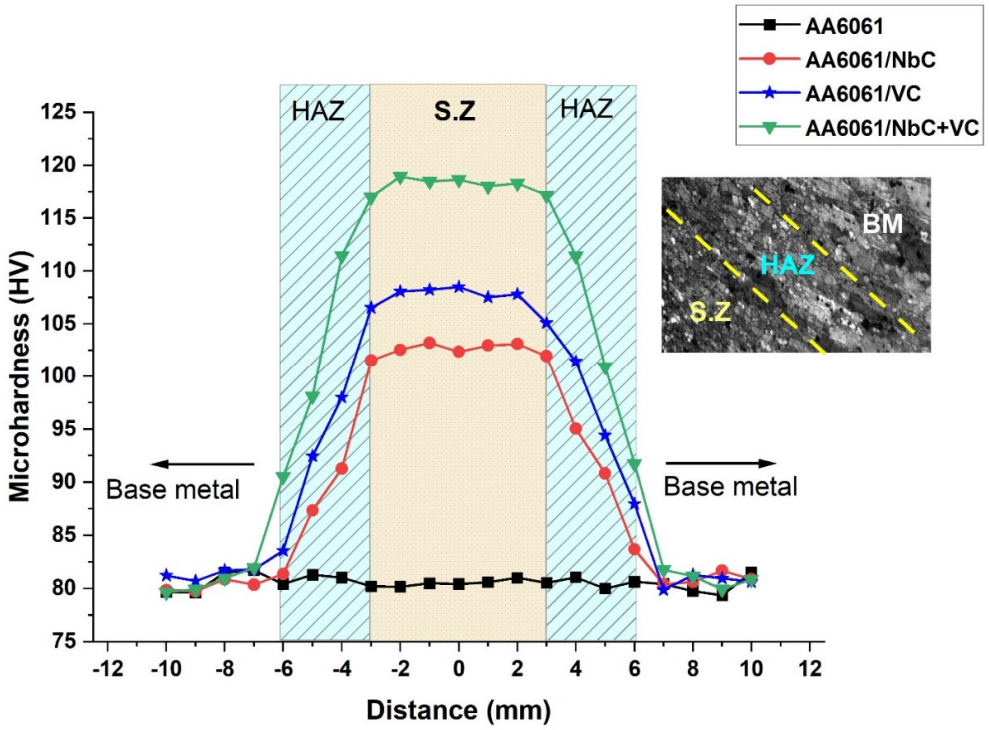


Figure 11. Microhardness, profile in the FSP, stirred zone, and heat-affected zone.

The overall improvement in the mechanical properties, compressive stress, yield stress, Young's modulus, and hardness of the manufactured composites are listed in Table 4. It is noted that incorporating hybrid particles (NbC, and Vc) improved all measured mechanical properties rather than reinforcing mono particles. The NbC recorded the lowest improvement than the VC.

4. Conclusions

In the current study, the mono and hybrid surface composite metal matrices were successfully fabricated using the FSP technique. The VC and NbC ceramic particles are used as reinforcement to improve the mechanical, microstructure, and physical properties and increase corrosion resistance.

The noticeable improvement in the mechanical properties of the composites containing hybrid reinforcement compared to those containing single particles is due to hybrid reinforcement enhancing the spatial configuration of each ceramic phase, which is very useful for the advantages of each ceramic individually.

The FSP and ceramic particles were used to improve the microstructure grain structure, which plays an essential role in restricting grain growth during the dynamic recrystallization process. Thus, for hybrid and mono-composite matrices, the grain size is decreased from 310 μm to an average of 10.5, 11.3, and 12 μm for the AA6061/NbC + VC, AA6061/VC, and AA6061/NbC respectively.

The hardness of the hybrid and mono composites AA6061/NbC + VC, AA6061/VC, and AA6061/NbC is greater than that of the base AA6061 alloy by 48.7%., 33.87%, and 27.3%, respectively. The enhancement in the hardness relies on the integration of the reinforcement particles and their good distribution inside the composite matrix.

The thermal expansion of surface composite matrices, in particular hybrid composite AA6061/NbC + VC, is effectively constrained, providing good enhancement for dimen-

sional stability of the Al alloy matrix, as evidenced by the fact that the CTE of reinforcements is lower than that of the base alloy.

These results indicate that the corrosion resistance of AA6061 and the composites increase with increasing exposure time, possibly due to partial passivation of the matrix alloy. The reduced weight loss of the composites with corrosion is further evidence that they were superior to the unreinforced Al alloy. Ceramic reinforcement particles of NbC and VC on the composite surface make it resistant to surface layer corrosion in an acidic environment.

Author Contributions: Conceptualization, E.B.M. and A.O.M.; methodology, E.B.M.; validation, M.A.T., and E.S.G.; formal analysis, A.O.M.; investigation, E.B.M.; writing—original draft preparation, E.B.M.; writing—review and editing, E.G.; supervision, E.B.M.; project administration, W.S.A.; funding acquisition, W.S.A. All authors have read and agreed to the published version of the manuscript.

Funding: This project was funded by the deanship of scientific research (DSR) at King Abdulaziz, under grant No. (RG-1-150-43).

Institutional Review Board Statement: Not applicable.

Informed Consent Statement: Not applicable.

Data Availability Statement: Not applicable.

Conflicts of Interest: The authors declare no conflict of interest.

References

1. Mussatto, A.; Ahad, I.U.; Mousavian, R.T.; Delaure, Y.; Brabazon, D. Advanced production routes for metal matrix composites. *Eng. Rep.* **2020**, *3*, e12330. [CrossRef]
2. Mussatto, A.; Groarke, R.; A-Hameed, A.; Ahad, I.U.; Vijayaraghavan, R.K.; O'Neill, A.; McNally, P.; Delaure, Y.; Brabazon, D. Evaluation via powder metallurgy of nano-reinforced iron powders developed for selective laser melting applications. *Mater. Des.* **2019**, *182*. [CrossRef]
3. Moustafa, E.B.; Taha, M.A. Preparation of high strength graphene reinforced Cu-based nanocomposites via mechanical alloying method: Microstructural, mechanical and electrical properties. *Appl. Phys. A* **2020**, *126*, 220. [CrossRef]
4. Rajak, D.K.; Pagar, D.D.; Kumar, R.; Pruncu, C.I. Recent progress of reinforcement materials: A comprehensive overview of composite materials. *J. Mater. Res. Technol.* **2019**, *8*, 6354–6374. [CrossRef]
5. Moustafa, E.B. Dynamic Characteristics Study for Surface Composite of AMMNCs Matrix Fabricated by Friction Stir Process. *Materials* **2018**, *11*, 1240. [CrossRef]
6. Abushanab, W.S.; Moustafa, E.B.; Harish, M.; Shanmugan, S.; Elsheikh, A.H. Experimental investigation on surface characteristics of Ti6Al4V alloy during abrasive water jet machining process. *Alex. Eng. J.* **2022**, *61*, 7529–7539. [CrossRef]
7. Nie, J.F.; Shin, K.S.; Zeng, Z.R. Microstructure, Deformation, and Property of Wrought Magnesium Alloys. *Metall. Mater. Trans. A* **2020**, *51*, 6045–6109. [CrossRef]
8. Moustafa, E.B.; Mosleh, A.O. Effect of (Ti–B) modifier elements and FSP on 5052 aluminum alloy. *J. Alloy. Compd.* **2020**, *823*, 153745. [CrossRef]
9. Moustafa, E.B.; AbuShanab, W.S.; Youness, R.A.; Taha, M.A. Improved mechanical properties of Cu8Ni4Sn alloy as functionally graded composites with preserving its thermal and electrical properties. *Mater. Chem. Phys.* **2022**, *292*, 126778. [CrossRef]
10. Moustafa, E.; Mohammed, S.; Abdel-Wanis, S.; Mahmoud, T.; El-Kady, E.S. Review multi pass friction stir processing. *Am. Acad. Sci. Res. J. Eng. Technol. Sci.* **2016**, *22*, 98–108.
11. Sharma, V.; Prakash, U.; Kumar, B.M. Surface composites by friction stir processing: A review. *J. Mater. Process. Technol.* **2015**, *224*, 117–134. [CrossRef]
12. Moustafa, E. Effect of Multi-Pass Friction Stir Processing on Mechanical Properties for AA2024/Al_2O_3 Nanocomposites. *Materials* **2017**, *10*, 1053. [CrossRef]
13. Rajendran, C.; Srinivasan, K.; Balasubramanian, V.; Balaji, H.; Selvaraj, P. Effect of tool tilt angle on strength and microstructural characteristics of friction stir welded lap joints of AA2014-T6 aluminum alloy. *Trans. Nonferrous Met. Soc. China* **2019**, *29*, 1824–1835. [CrossRef]
14. Reza-E-Rabby, M.; Tang, W.; Reynolds, A. Effect of Tool Pin Features and Geometries on Quality of Weld During Friction Stir Welding. In *Friction Stir Welding and Processing VII*; Mishra, R., Mahoney, M.W., Sato, Y., Hovanski, Y., Verma, R., Eds.; Springer International Publishing: Cham, Switzerland, 2016; pp. 163–171.
15. Mehdi, H.; Mishra, R. Effect of friction stir processing on mechanical properties and heat transfer of TIG welded joint of AA6061 and AA7075. *Def. Technol.* **2020**, *17*, 715–727. [CrossRef]

16. Wu, B.; Ibrahim, M.; Raja, S.; Yusof, F.; Razak, B.B.A.; Bin Muhamad, M.R.; Huang, R.; Zhang, Y.; Badruddin, I.A.; Hussien, M.; et al. The influence of reinforcement particles friction stir processing on microstructure, mechanical properties, tribological and corrosion behaviors: A review. *J. Mater. Res. Technol.* **2022**, *20*, 1940–1975. [CrossRef]
17. Aziz, S.S.A.; Abulkhair, H.; Moustafa, E.B. Role of hybrid nanoparticles on thermal, electrical conductivity, microstructure, and hardness behavior of nanocomposite matrix. *J. Mater. Res. Technol.* **2021**, *13*, 1275–1284. [CrossRef]
18. Moustafa, E.B.; Melaibari, A.; Alsoruji, G.; Khalil, A.M.; Mosleh, A.O. Tribological and mechanical characteristics of AA5083 alloy reinforced by hybridising heavy ceramic particles Ta2C & VC with light GNP and Al2O3 nanoparticles. *Ceram. Int.* **2021**, *48*, 4710–4721. [CrossRef]
19. Mehta, K.; Badheka, V. Wear behavior of boron-carbide reinforced aluminum surface composites fabricated by Friction Stir Processing. *Wear* **2019**, *426-427*, 975–980. [CrossRef]
20. Kumar, M.S.; Vasumathi, M.; Begum, S.R.; Luminita, S.M.; Vlase, S.; Pruncu, C.I. Influence of B4C and industrial waste fly ash reinforcement particles on the micro structural characteristics and mechanical behavior of aluminium (Al–Mg–Si-T6) hybrid metal matrix composite. *J. Mater. Res. Technol.* **2021**, *15*, 1201–1216. [CrossRef]
21. Manivannan, A.; Sasikumar, R. Fabrication and Characterization of Aluminium Boron Nitride Composite for Fins. *Mater. Today: Proc.* **2018**, *5*, 8618–8624. [CrossRef]
22. Moustafa, E.B.; Mikhaylovskaya, A.V.; Taha, M.A.; Mosleh, A.O. Improvement of the microstructure and mechanical properties by hybridizing the surface of AA7075 by hexagonal boron nitride with carbide particles using the FSP process. *J. Mater. Res. Technol.* **2022**, *17*, 1986–1999. [CrossRef]
23. Boopathi, S.; Jeyakumar, M.; Singh, G.R.; King, F.L.; Pandian, M.; Subbiah, R.; Haribalaji, V. An experimental study on friction stir processing of aluminium alloy (AA-2024) and boron nitride (BNp) surface composite. *Mater. Today Proc.* **2022**, *59*, 1094–1099. [CrossRef]
24. Kumar, T.S.; Shalini, S.; Kumar, K.K. Effect of friction stir processing and hybrid reinforcement on wear behaviour of AA6082 alloy composite. *Mater. Res. Express* **2020**, *7*, 026507. [CrossRef]
25. Lin, G.-M.; Xie, G.-Y.; Sui, G.-X.; Yang, R. Hybrid effect of nanoparticles with carbon fibers on the mechanical and wear properties of polymer composites. *Compos. Part B Eng.* **2012**, *43*, 44–49. [CrossRef]
26. Moustafa, E.B. Hybridization effect of BN and Al2O3 nanoparticles on the physical, wear, and electrical properties of aluminum AA1060 nanocomposites. *Appl. Phys. A* **2021**, *127*, 724. [CrossRef]
27. Moustafa, E.B.; Melaibari, A.; Alsoruji, G.; Khalil, A.M.; Mosleh, A.O. Al 5251-based hybrid nanocomposite by FSP reinforced with graphene nanoplates and boron nitride nanoparticles: Microstructure, wear, and mechanical characterization. *Nanotechnol. Rev.* **2021**, *10*, 1752–1765. [CrossRef]
28. Peng, Y.; Zhao, H.; Ye, J.; Yuan, M.; Tian, L.; Li, Z.; Liu, Y.; Chen, J. 3D multiscale tri-level finite element analysis of aluminum matrix composites with Nano & Micro hybrid inclusions. *Compos. Struct.* **2023**, *305*, 116545. [CrossRef]
29. Muzeer, S.; Sivaganesan, S. Sivaganesan, Tribological behaviour of aluminium based hybrid metal matrix composites (Al6061/B_4C/ZrO_2/SiC). *Mater. Today Proc.* **2022**, *56*, 507–513.
30. Jayavelu, S.; Mariappan, R.; Rajkumar, C. Wear characteristics of sintered AA2014 with alumina and titanium di-Boride metal matrix composites. *Int. J. Ambient. Energy* **2018**, *42*, 173–178. [CrossRef]
31. Moustafa, E.B.; Melaibari, A.; Basha, M. Wear and microhardness behaviors of AA7075/SiC-BN hybrid nanocomposite surfaces fabricated by friction stir processing. *Ceram. Int.* **2020**, *42*, 173–178. [CrossRef]
32. Paidar, M.; Ojo, O.O.; Ezatpour, H.R.; Heidarzadeh, A. Influence of multi-pass FSP on the microstructure, mechanical properties and tribological characterization of Al/B4C composite fabricated by accumulative roll bonding (ARB). *Surf. Coatings Technol.* **2019**, *361*, 159–169. [CrossRef]
33. Zayed, A.S.; Kamel, B.M.; Abdelsadek Osman, T.; Elkady, O.A.; Ali, S. Experimental study of tribological and mechanical properties of aluminum matrix reinforced by Al2O3/CNTs. *Fuller. Nanotub. Carbon Nanostructures* **2019**, *27*, 538–544. [CrossRef]
34. Shyu, R.; Ho, C. In situ reacted titanium carbide-reinforced aluminum alloys composite. *J. Mater. Process. Technol.* **2006**, *171*, 411–416. [CrossRef]
35. Williams, W.S. Transition-metal carbides. *Prog. Solid State Chem.* **1971**, *6*, 57–118. [CrossRef]
36. Moustafa, E.B.; Abushanab, W.S.; Melaibari, A.; Yakovtseva, O.; Mosleh, A.O. The Effectiveness of Incorporating Hybrid Reinforcement Nanoparticles in the Enhancement of the Tribological Behavior of Aluminum Metal Matrix Composites. *Jom* **2021**, *73*, 4338–4348. [CrossRef]
37. Rajabi, A.; Ghazali, M.J.; Daud, A.R. Chemical composition, microstructure and sintering temperature modifications on mechanical properties of TiC-based cermet–A review. *Mater. Des.* **2015**, *67*, 95–106. [CrossRef]
38. Wolf, W.; Bolfarini, C.; Kiminami, C.S.; Botta, W.J. Recent developments on fabrication of Al-matrix composites reinforced with quasicrystals: From metastable to conventional processing. *J. Mater. Res.* **2021**, *36*, 281–297. [CrossRef]
39. Mahran, G.M.A.; Omran, A.-N.M. Grain Refining of Aluminium and 6063 Alloys Using Al-V Alloy Containing Al3V Intermetallic Compound. *Mater. Sci.* **2021**, *28*, 41–47. [CrossRef]
40. Roduit, N.J. Image Analysis Toolbox for Measuring and Quantifying Components of High-Definition Images 1.3.1. 2019. Available online: https://jmicrovision.github.io (accessed on 5 April 2019).
41. Murugesan, R.; Gopal, M.; Murali, G. Effect of Cu, Ni addition on the CNTs dispersion, wear and thermal expansion behavior of Al-CNT composites by molecular mixing and mechanical alloying. *Appl. Surf. Sci.* **2019**, *495*, 143542. [CrossRef]

42. Okumus, S.C.; Aslan, S.; Karslioglu, R.; Gultekin, D.; Akbulut, H. Thermal Expansion and Thermal Conductivity Behaviors of Al-Si/SiC/graphite Hybrid Metal Matrix Composites (MMCs). *Mater. Sci.* **2012**, *18*, 341–346. [CrossRef]
43. Sridhar, R. Durability study on engineered cementitious composites with hybrid fibers under sulfate and chloride environments. *Clean. Mater.* **2022**, *5*, 100121. [CrossRef]
44. Tharanikumar, L.; Mohan, B.; Anbuchezhiyans, G. Enhancing the Microstructure and Mechanical properties of Si3N4- BN strengthened Al-Zn-Mg Alloy Hybrid Nano Composites using vacuum assisted stir casting method. *J. Mater. Res. Technol.* **2022**, *20*, 3646–3655. [CrossRef]
45. Alzahrani, M.A.; Moustafa, E.B.; Alsoruji, G.; Mosleh, A.O. The influence of the modifying elements on the microstructure, mechanical, and deformation properties of aluminum alloys. *Front. Mater.* **2022**, *9*, 1100566. [CrossRef]
46. Kumar, K.R.; Pridhar, T.; Balaji, V.S. Mechanical properties and characterization of zirconium oxide (ZrO_2) and coconut shell ash(CSA) reinforced aluminium (Al 6082) matrix hybrid composite. *J. Alloy. Compd.* **2018**, *765*, 171e179.
47. John, C.F.; Paul, R.C.; Singh, S.C.E.; Jacobjose, J.; Ramkumar, T.; Hikku, G.S.; Sharma, R.K.; Sengottuvel, P. Corrosion resistance on Al-12Si-xZrC composites using acid mediums. *Int. J. Mech. Mechatron. Eng.* **2017**, *17*, 67–74.
48. Thapliyal, S.; Dwivedi, D.K. Barium titanate reinforced nickel aluminium bronze surface composite by friction stir processing. *Mater. Sci. Technol.* **2018**, *34*, 366–377. [CrossRef]
49. Ma, Z.; Zhou, Y.; Long, S.; Lu, C. An Inverse Approach for Extracting Elastic–plastic Properties of Thin Films from Small Scale Sharp Indentation. *J. Mater. Sci. Technol.* **2012**, *28*, 626–635. [CrossRef]

Disclaimer/Publisher's Note: The statements, opinions and data contained in all publications are solely those of the individual author(s) and contributor(s) and not of MDPI and/or the editor(s). MDPI and/or the editor(s) disclaim responsibility for any injury to people or property resulting from any ideas, methods, instructions or products referred to in the content.